X-615-65-185

NASA TMX-55216

ROCKET MEASUREMENTS OF COSMIC NOISE INTENSITIES BELOW 5 Mc/s

BY
J. K. ALEXANDER
R. G. STONE

APRIL 1965

NASA — GODDARD SPACE FLIGHT CENTER
GREENBELT, MARYLAND

Radio Astronomy Section Reprint

ROCKET MEASUREMENTS OF COSMIC NOISE INTENSITIES BELOW 5 MC/S

J. K. Alexander and R. G. Stone
NASA-Goddard Space Flight Center

ABSTRACT

23915

Cosmic radio noise intensities at four frequencies below 5 Mc/s were measured with a rocket probe launched from Wallops Island, Va., on 23 October 1964. The experimental payload which consisted of a short dipole antenna, four TRF receivers, a reference noise source and an antenna impedance probe reached an apogee altitude of 1070 km during the 20-minute flight. The measured cosmic background noise intensities were

$(2.2 \,^{+\,0.9}_{-\,0.6}) \times 10^{-20}$ w/m^2/cps/sr. at 1.91 Mc/s,

$(2.7 \pm 0.5) \times 10^{-20}$ w/m^2/cps/sr. at 2.85 Mc/s,

$(1.7 \,^{+\,1.1}_{-\,0.7}) \times 10^{-20}$ w/m^2/cps/sr. at 3.60 Mc/s,

$(2.2 \,^{+\,1.4}_{-\,0.9}) \times 10^{-20}$ w/m^2/cps/sr. at 4.70 Mc/s.

These results, which are for a hemisphere centered near the North Galactic Pole, are not inconsistent with an interpretation of the turn-over in the noise spectrum below 5 Mc/s as being due to absorption by nearby galactic HII regions having an emission measure the order of 5 cm^{-6} pc.

The anomalous radio noise enhancements observed at low altitudes (where $1-Y^2<X<1$, $Y<1$) on this and other similar experiments are shown to be associated with resonance effects in the antenna impedance in the ionospheric plasma. Author

INTRODUCTION

Since radio astronomical measurements are severely hampered by the ionosphere at frequencies below about 10 Mc/s, observations in this frequency range must be performed with high altitude rocket probes or satellites. There have been some ground-based observations under very special conditions (Ellis, 1964), but this approach is quite difficult at best. This concern is born out by the results of recent space-borne experiments which are not entirely consistent with the measurements of cosmic noise intensities below 5 Mc/s obtained from the ground. Rocket probe measurements of the average cosmic noise intensities at 1.225 and 2.0 Mc/s by Walsh et al (1963) agree with the suggestion by Ellis and co-workers that the radio spectrum falls off sharply in this range, although the rocket intensities are nearly twice the intensities derived from the ground observations. A high altitude rocket measurement by Huguenin et al (1963) at 2.2 Mc/s agrees more closely with the ground-based results, but the experimental uncertainty in the rocket data is too large to help resolve the discrepancy between the other rocket and ground observations. Alouette satellite measurements reported by Hartz (1964), on the other hand, suggest that the cosmic noise spectrum between 1.5 and 5 Mc/s is flatter than observed by either Ellis or Walsh et al.

In order that this situation might be resolved to provide a more consistent picture of the cosmic noise spectrum, a radio astronomy rocket probe was launched to an altitude of nearly 1100 km above Wallops Island, Virginia, on October 23, 1964. The payload was instrumented to measure average noise intensities at 1.91, 2.85, 3.60 and 4.70 Mc/s. A report of this experiment and a discussion of the implications of its results follow.

EXPERIMENT INSTRUMENTATION

The radio astronomy instrumentation was comprised of a

short (9.76m) dipole antenna which was connected through appropriate matching networks to four TRF receivers plus a comparison noise source and a probe to measure antenna impedance. A pair of orthogonal magnetometers and a solar aspect sensor provided supporting information regarding vehicle spin and aspect. A block diagram of the experiment is given in Figure 1.

The telescoping dipole was initially folded under the payload nose cone and was then erected to its full length after 130 seconds of flight at an altitude of about 225 km. An internal programmer alternately connected the antenna to the input of the receiving system and to the input terminals of the impedance probe. As shown in Figure 1, the receivers were operated in pairs so that when one pair of receivers was sampling the antenna (e.g., at 1.91 and 3.60 Mc/s) the other pair (2.85 and 4.70 Mc/s) was connected to the comparison noise source for calibration. The comparison noise source, in turn, was programmed to provide three levels of calibration - a zero level, a level near the middle of the receiver dynamic range, and a high level signal. The full program sequence is given in Figure 2. For the first 15 seconds of the duty cycle the receivers alternately sample the antenna and the noise source in 2.5-second intervals. For the final 5 seconds of the program cycle the antenna impedance probe is on, and the receivers are inoperative.

Each receiver employed seven stages of wide-band amplification and passive band-pass filters to determine the center frequency and bandwidth. The noise bandwidths for each radiometer system, including the matching networks, were 34 kc/s at 1.91 Mc/s, 260 kc/s at 2.85 Mc/s, 185 kc/s at 3.60 Mc/s, and 190 kc/s at 4.70 Mc/s. Each channel had a wideband output which utilized the full available telemetry bandwidth and a narrow-band output which had a time constant of 0.14 second.

The noise source consisted of a Solitron SD2L noise diode and two broad-band amplifier stages. A three-step attenuator was switched by relays to provide three levels of calibration to the receivers. To improve the stability of the noise source, power was never removed during the flight. Instead, the last step of the attenuator terminated the radiometers to obtain a residual ("zero") noise level.

A schematic diagram of the antenna impedance probe is given in Figure 3. A one-volt rms signal at the frequency of interest (either 2.00, 2.85, 4.44 or 5.47 Mc/s) is applied to the antenna through a wide-band transformer. A sample of the voltage, V, across the antenna and the current, I, in the antenna at frequency, f, are obtained from the sensor at the antenna terminals. These are individually mixed with a signal from a beat-frequency-oscillator at frequency, $f-\Delta f$, and the signals at the difference frequency, Δf, are filtered, amplified and detected to provide dc outputs proportional to $|V|$ and $|I|$. The two signals are also compared in a phase detector to provide an output proportional to the phase angle, ϕ. Since the antenna has a very high capacitive reactance and a very small resistance, an expander is also utilized to give a fine output for phase angles near -90°.

Since the calibration of an experiment of this type is of considerable importance, we will briefly describe the calibration procedures employed for our payload. As shown in Figure 4 a, the output of a calibration noise generator was fed through a 1:1 balun to an R-C network which simulated the impedance of the dipole antenna used in flight. The reactance of the dummy antenna could be varied over a wide range (corresponding to a range of antenna capacitance from zero to twice the free space value) in order that the mismatch caused by ionospheric detuning could be measured. The

output of the flight radiometers was delivered to the flight telemetry and was then recorded by standard telemetry ground station equipment. Hence, the full experimental payload was calibrated in the flight configuration. The receiving system was calibrated over a wide range of temperatures, supply voltages, and values of antenna impedance, and the temperature and supply voltage of each sub-system was later monitored during the flight so that appropriate corrections could be made during data analysis if necessary. The antenna impedance probe was calibrated simultaneously.

The calibration noise source was composed of an SD2L zener diode followed by a wide-band amplifier and a variable precision attenuator. To determine its output reliably, the noise source was compared with a CW signal generator as shown in Figure 4b. The signal generator output at a fixed level was first measured to an accuracy of ±2 percent with a broad-band calorimeter. (The calorimeter was not sufficiently sensitive to measure the noise source output directly.) Then the signal generator and noise source outputs were compared using a communications receiver and a VTVM. It can be shown that, for a narrow band receiver with a linear envelope detector and a DC meter, the ratio of the input noise power to the input CW power is equal to $4/\pi$ for a given VTVM reading.

EXPERIMENTAL RESULTS

The experiment was launched on a four-stage Javelin rocket at 16^h 00.6^m U.T. on October 23, 1964, and reached an apogee altitude of 1070 km after about 10.5 minutes of flight.

Good data were obtained from antenna deployment at about 225 km altitude until the payload re-entered the ionosphere at about 200 km altitude. The vehicle was above 1000 km for about 5 minutes, and only noise data obtained during this

period were used for the cosmic noise intensity analysis. The Explorer XX topside-sounder satellite passed directly over Wallops Island about 20 minutes before launch, and the sounder data showed the local electron plasma frequency at 1000 km to be less than 850 kc/s.

The raw noise data in the form of receiver output voltages for each frequency are plotted in Figure 5. The vertical scales have been displaced for easier inspection, and hence the relative noise values from frequency-to-frequency have not been accurately preserved. Notice that at the lowest frequency (1.91 Mc/s) the receiver output begins at a relatively low level and then increases sharply to a peak at about 600 km altitude. After falling abruptly in about 30 seconds, the apparent noise level then shows a gradual rise to a plateau centered about flight apogee. As the vehicle descends the pattern is repeated in reverse - a gradual decrease, then a sharp noise enhancement, and finally a decline to a low level at altitudes below 400 km. Each data point in Figure 5 represents an average value for each 2.5-second sampling interval. The noise output was actually strongly spin-modulated below about 700 km, although no clear evidence for spin modulation could be detected when the payload was much above that altitude. The uncertainty in the telemetry system and in data reading is shown by the error flags. At 2.85 Mc/s the general variation of noise level with altitude was the same except that the noise enhancement peak occurred at a lower altitude. This trend is further verified by the 3.6 and 4.7 Mc/s data. The 3.6 Mc/s noise enhancement was observed to begin immediately after antenna deployment before the corresponding events at 2.85 and 1.91 Mc/s and after the lower frequency events at the end of the flight. At 4.7 Mc/s, only the end of the enhancement event appears to have been

observed during ascent, and there is no indication of an enhancement on the descending leg of the flight. Notice that the observed signal level was extremely steady at 3.6 and 4.7 Mc/s throughout the eleven-minute period when the vehicle was above 700 km.

For comparison with the general features of the noise data, the impedance probe results at 2.0 and 4.4 Mc/s are plotted as a function of time in Figure 6. At 2.0 Mc/s, the antenna resistance appears to be extremely high at altitudes below 600 km, shows strong modulation above a value 30 to 40 times the free space resistance in the 700 to 900 km region, and tapers off to a value close to the free space resistance above 1000 km. The 2.0 Mc/s antenna capacitance, on the other hand, goes from zero near 600 km smoothly up to its free space value at apogee. There is evidence for spin modulation of the capacitance at the lower altitudes, but this effect cannot be clearly delineated since the impedance probe sampling rate is close to the vehicle spin rate. At 4.4 Mc/s, the apparent antenna resistance was unexpectedly large below 500 km although it rapidly returned to its free space value at high altitudes. The capacitance at 4.4 Mc/s followed the same pattern as at 2.0 Mc/s. The error bars shown for the data in Figure 6 represent the total estimated uncertainty of the impedance probe and are ±4 ohms and ±0.5 pf at 2.0 Mc/s and ±1.7 ohms and ±0.25 pf at 4.4 Mc/s for relative measurements of resistance and capacitance, respectively. The precision in absolute measurement may be somewhat less. The detailed impedance behavior at low altitudes will be discussed in relation to the noise enhancement regions in a subsequent section of this report.

Using the antenna impedance values measured in flight, the receiver data obtained at altitudes above 1000 km have

been converted into cosmic noise intensities at each frequency. They are

$$(2.2 \begin{smallmatrix} + 0.9 \\ - 0.6 \end{smallmatrix}) \times 10^{-20} \text{w/m}^2\text{/cps/sr. at 1.91 Mc/s,}$$

$$(2.7 \pm 0.5) \times 10^{-20} \text{w/m}^2\text{/cps/sr. at 2.85 Mc/s,}$$

$$(1.7 \begin{smallmatrix} + 1.1 \\ - 0.7 \end{smallmatrix}) \times 10^{-20} \text{w/m}^2\text{/cps/sr. at 3.60 Mc/s,}$$

$$(2.2 \begin{smallmatrix} + 1.4 \\ - 0.9 \end{smallmatrix}) \times 10^{-20} \text{w/m}^2\text{/cps/sr. at 4.70 Mc/s.}$$

The uncertainty estimates include the possible errors in the radiometer system calibration, telemetry system and data reading, and instrumentation performance in flight. The intensity measurements at 1.91 and 2.85 Mc/s are the most reliable and have an uncertainty of ±1.5 db and $\begin{smallmatrix} +0.8 \\ -0.9 \end{smallmatrix}$ db, respectively. Due to a nonlinearity in the receiver response curves at 3.60 and 4.70 Mc/s, however, these measurements must carry an uncertainty greater than ±2 db.

Before going on to a discussion of the implications of the cosmic noise intensity measurements we will describe in more detail the low altitude noise enhancements and anomalous impedance effects. Plotted in Figure 7 are 1.91 Mc/s relative apparent noise intensity in the form of receiver output voltage, 2.0 Mc/s antenna reactance, and 2.0 Mc/s antenna resistance for altitudes between 300 and 800 km. Notice that directly associated with the noise peaks is a reversal in the sign of the reactance, from inductive at the low altitude side to capacitive above, and a peak in the resistance at a value of several thousand ohms. The same effect is seen in the data at 2.85 Mc/s as plotted in Figure 8.

The noise enhancements have been observed previously on the rocket flights of both the University of Michigan (Walsh et al, 1963) and Harvard University (Huguenin et al, 1963),

and these workers have identified the events with the magneto-ionic regions defined by $1-Y^2<X<1$ and $Y<1$. This is approximately the case for our data. Within the limits to which the variation of electron density with height are know, the noise enhancements begin at X=1 during ascent and end at X=1 on descent. The high altitude limit appears to be nearer to $X=1-Y$ than $X=1-Y^2$, however. There is evidence that each noise level enhancement is actually split into a pair of peaks; however this effect does not appear in the impedance data. Nevertheless the noise level enhancements and the resonance effects in the antenna impedance appear to be closely related.

Although it is tempting at first glance to explain the noise peaks in terms of genuinely high ionospheric noise fields produced by "plasma waves", it is difficult to conceive of the energy source required in this interpretation. The impedance data, however, provide evidence which supports a different interpretation of the high noise levels. Since the antenna resistance goes as high as several thousand ohms in this magneto-ionic region the antenna will appear to be a much more efficient radiator, and the apparent noise power received will increase. The 2 Mc/s antenna temperature in this region was calculated to be the order of 10^5 ^oK. Although this is two orders of magnitude above the kinetic temperature of the ionospheric plasma, it could be accounted for in terms of a strongly absorbed cosmic brightness temperature of about 10^7 ^oK.

The unexpectedly high values of antenna resistance at 2.0 Mc/s which are observed even at altitudes above the noise enhancement regions are more puzzling. This affect does not appear to be reflected in the noise measurements. Since an oscillator excites the antenna during the impedance measurements, the antenna is no longer a passive device as in the receiving mode. It seems possible that the RF voltage on the

antenna could interact with the ion sheath about the antenna to produce nonlinear plasma waves when the impedance probe is energized. This effect could then be observed as resistive loading of the antenna and could possibly produce the high resistance values observed at 2 Mc/s. Certainly the whole problem of antenna impedance in the ionosphere deserves more detailed experimental study.

DISCUSSION

The observed cosmic noise intensities are plotted in Figure 9 along with other measurements of the noise spectrum in this frequency range. Since our measurements refer to the hemisphere centered at about $l_{II}=100^{o}$, $b_{II}=80^{o}$, we have plotted the curve from the Alouette satellite measurements by Hartz (1964) for the North Galactic halo region. Since Alouette is at an altitude of about 1000 km these measurements should be comparable, and there is agreement within the uncertainties of the two sets of measurements. The data obtained from the ground by Ellis (1964) are for the region of the South Galactic pole, but were obtained with a more directive antenna than the space-borne experiments. The measurements of Walsh et al (1963) are for a hemisphere centered on $l_{II}=144^{o}$, $b_{II}= -19^{o}$, whereas the observations by Huguenin et al (1963) represent an average over nearly the whole celestial sphere. Both the measurements from the ground and from the Michigan rocket suggest that the cosmic noise spectrum has begun to fall of sharply in the neighborhood of 2 Mc/s, and this has been widely interpreted to be due to free-free absorption in ionized galactic hydrogen having an emission measure, $\langle N_e^2 L \rangle$, of about 4 to 6 pc cm^{-6}. The new measurements at 1.91, 2.85, 3.60 and 4.70 Mc/s are consistent with that interpretation.

The rocket and satellite measurements have been re-

plotted in Figure 10 for comparison with a straight line extrapolation of the spectrum observed at high frequencies as shown by the dashed line. The background intensity has been taken to vary as $f^{-0.6}$ in this extrapolation. If one then assumes that there is uniform absorption by HII, then the observed intensity will be

$$I \cong I_o \exp\left(\frac{-0.17}{f^2} \int \frac{N_e^2}{T^{3/2}}\, dl\right)$$

$$\cong I_o \exp\left[\frac{-0.17}{f^2 T^{3/2}} \langle N_e^2 L\rangle\right]$$

For a temperature $T = 10^4$ ^oK and an emission measure $\langle N_e^2 L\rangle = 5 cm^{-6} pc$, one would expect to observe the spectrum shown by the solid curve, and indeed it is a good fit to the observed points. Detailed interpretations of the spectrum on the basis of the observations made to date should be considered with caution, however, since the large uncertainties on most measurements embrace a rather wide range of spectral shapes.

CONCLUSIONS

Measurements of integrated cosmic noise intensities for a hemisphere centered near the North Galactic Pole have shown the spectrum to have a broad peak near 3 Mc/s at an intensity of about $2.7 \times 10^{-20} w/m^2/cps/sr$. These results are not inconsistent with the concept of absorption by a uniform HII region in the solar neighborhood having an emission measure of 5 pc cm^{-6}. The shape of the spectrum below 5 Mc/s may give an indication of the degree of uniformity or the clumpiness of the ionized hydrogen, but the uncertainties in the present measurements do not make this possible. Observations with a directive antenna below 10 Mc/s will clarify

this situation in considerable detail, and experiments of this nature are being planned (Alexander and Stone, 1964). In the meantime, there are at least three experimental areas which can contribute to solution of the problem. They are:

(1) one or two intensity measurements below 1 Mc/s,

(2) measurements with improved accuracy between 1 and 10 Mc/s,

(3) measurements with some directivity between 10 and 20 Mc/s to facilitate extrapolation of the spectrum from high to low frequencies.

Measurements of the impedance of a short dipole in the ionospheric plasma have been interpreted to show at least two different phenomena which deserve further study. The first is the apparent noise enhancement in the region between $X=1$ and $X=1-Y^2$ accompanied by a peak in antenna resistance which has the effect of increasing its efficiency. The second is the high value of antenna resistance observed when it is excited in the region for $X<1-Y^2$, $Y<1$. The latter effect, which may also occur to a different degree for $X>1-Y^2$, may be due to resistive loading of the antenna by nonlinear interaction with the plasma sheath surrounding the antenna. These problems will be discussed in detail in another paper.

ACKNOWLEDGEMENTS

The authors gratefully acknowledge the contributions of Marc Chomet and his associates of Airborne Instruments Laboratory who developed and calibrated the flight radiometric systems and A. D. Parsons, T. Tepper, and their associates of Electromagnetic Research Corporation who developed the antenna

impedance probe. Data from bottomside ionospheric soundings at Wallops Island and topside ionospheric soundings by Explorer XX were kindly provided by the NBS Central Radio Propagation Laboratory.

REFERENCES

Alexander, J. K. and Stone, R. G. Ann.d'Astrophys. 27, 837 (1964).

Ellis, G. R. A., Nature 204, 171 (1964).

Hartz, T. R., Ann.d'Astrophys., 27, 823 (1964).

Huguenin, G. R., Lilley, A. E., McDonough, W. H., and Papagiannis, M. D., Harvard College Observatory Rpt. HSRP-107 (1963).

Walsh, D., Haddock, F. T., and Schulte, H. F., COSPAR, 6th Plenary Meeting, Warsaw (1963).

FIGURE CAPTIONS

Figure 1 - Block Diagram of Radio Astronomy Payload.

Figure 2 - Program Sequence for Radio Astronomy Experiment.

Figure 3 - Block Diagram of Antenna Impedance Probe.

Figure 4a- Payload Calibration Diagram.
b- Calibration of Standard Noise Source.

Figure 5 - Variation of Relative Noise Intensity with Time and Altitude.

Figure 6 - Variation of Antenna Impedance with Time and Altitude.

Figure 7 - Comparison of 1.91 Mc/s Noise Enhancement Events with Antenna Impedance at 2.0 Mc/s.

Figure 8 - Comparison of 2.85 Mc/s Noise Enhancement Events with Antenna Impedance at 2.85 Mc/s.

Figure 9 - Observed Cosmic Noise Intensities Below 10 Mc/s.

Figure 10 - Comparison of Rocket and Satellite Measurements with Predicted Spectrum for Uniform HII Absorption.

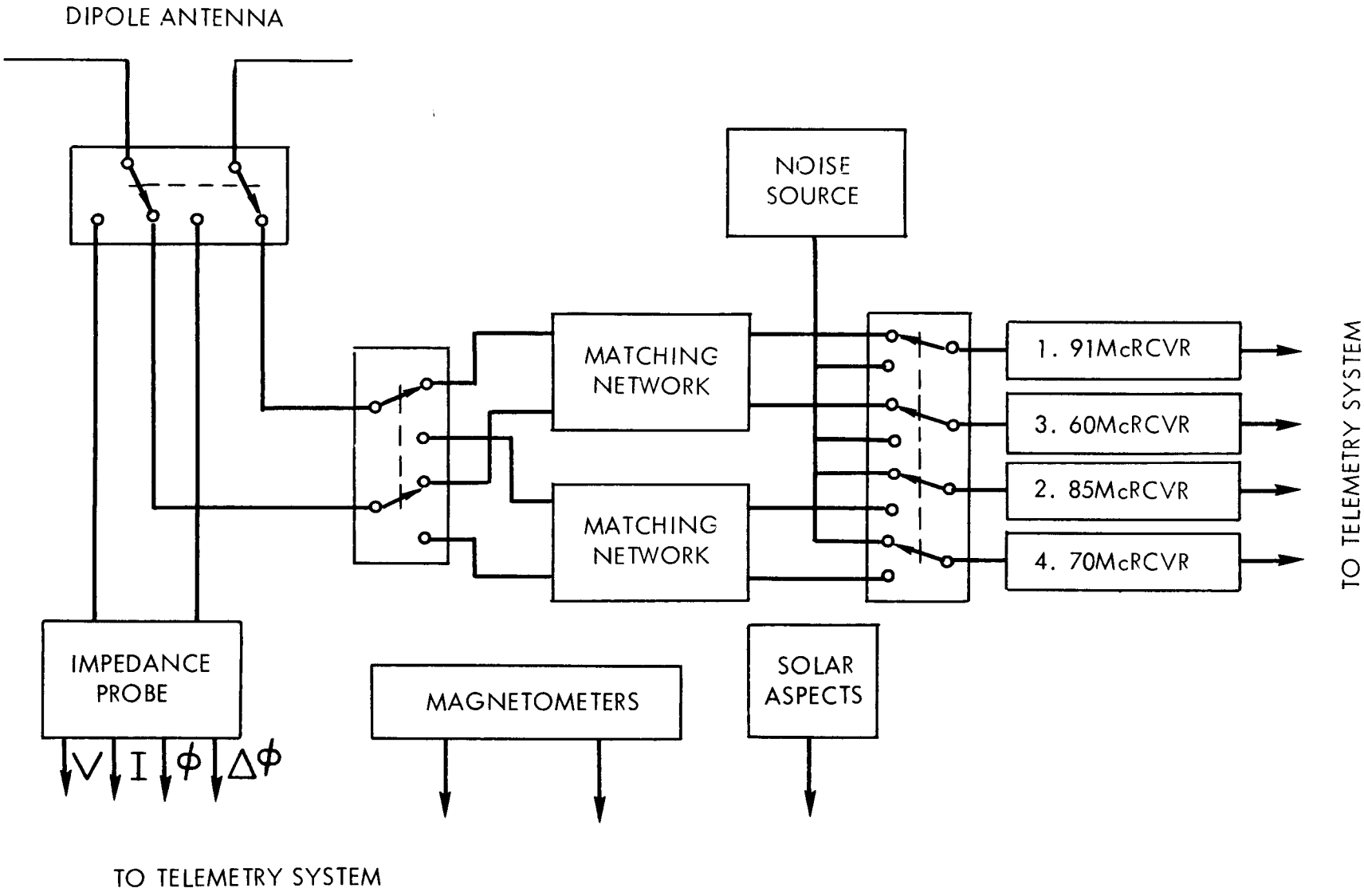
DIPOLE ANTENNA
NOISE SOURCE
MATCHING NETWORK
MATCHING NETWORK
1. 91McRCVR
3. 60McRCVR
2. 85McRCVR
4. 70McRCVR
TO TELEMETRY SYSTEM
IMPEDANCE PROBE
V I ϕ Δϕ
MAGNETOMETERS
SOLAR ASPECTS
TO TELEMETRY SYSTEM

Figure 1

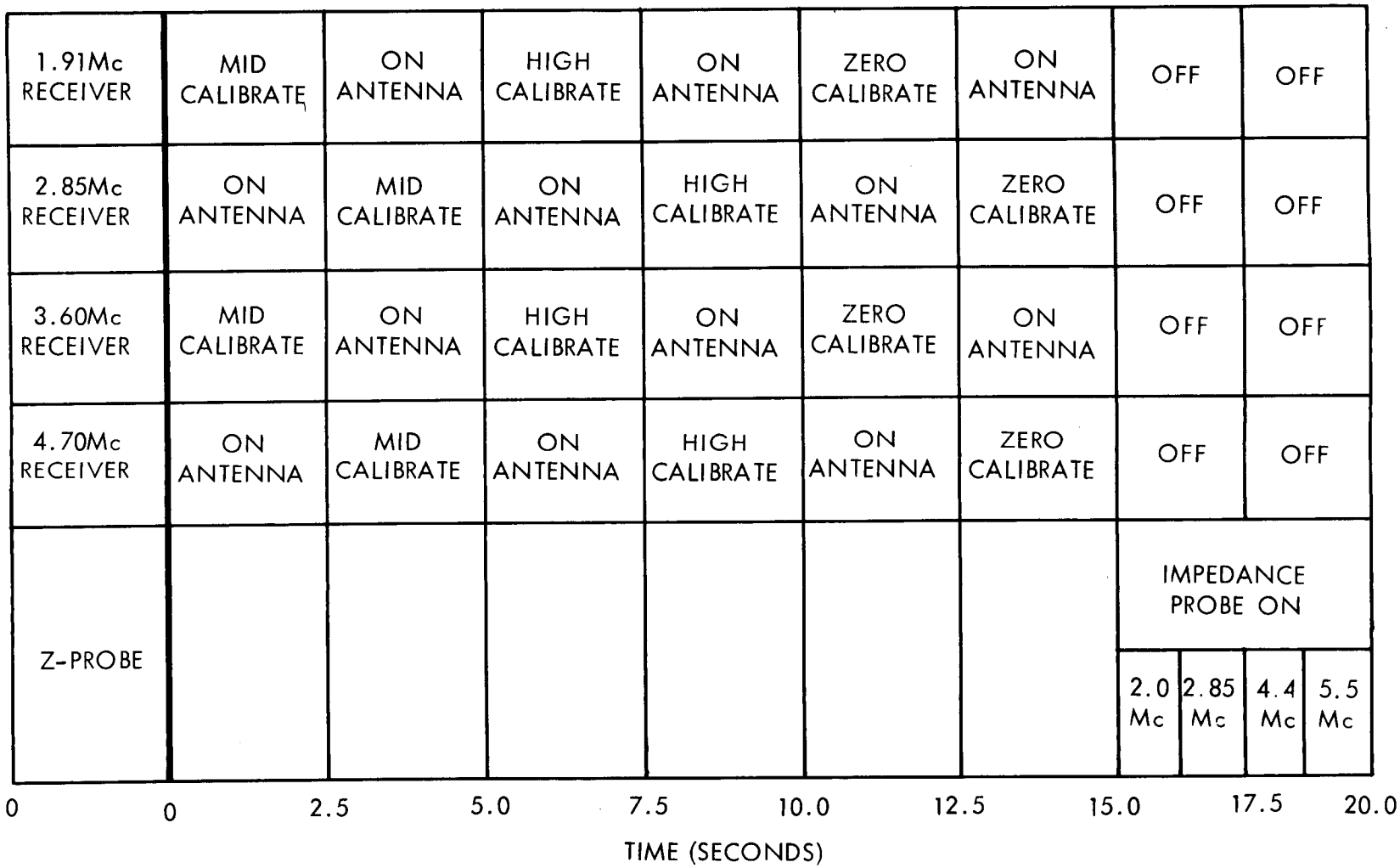
1.91Mc RECEIVER
MID CALIBRATE
ON ANTENNA
HIGH CALIBRATE
ON ANTENNA
ZERO CALIBRATE
ON ANTENNA
OFF
OFF
2.85Mc RECEIVER
ON ANTENNA
MID CALIBRATE
ON ANTENNA
HIGH CALIBRATE
ON ANTENNA
ZERO CALIBRATE
OFF
OFF
3.60Mc RECEIVER
MID CALIBRATE
ON ANTENNA
HIGH CALIBRATE
ON ANTENNA
ZERO CALIBRATE
ON ANTENNA
OFF
OFF
4.70Mc RECEIVER
ON ANTENNA
MID CALIBRATE
ON ANTENNA
HIGH CALIBRATE
ON ANTENNA
ZERO CALIBRATE
OFF
OFF
Z-PROBE
IMPEDANCE PROBE ON
2.0 Mc
2.85 Mc
4.4 Mc
5.5 Mc
0
0
2.5
5.0
7.5
10.0
12.5
15.0
17.5
20.0
TIME (SECONDS)

Figure 2

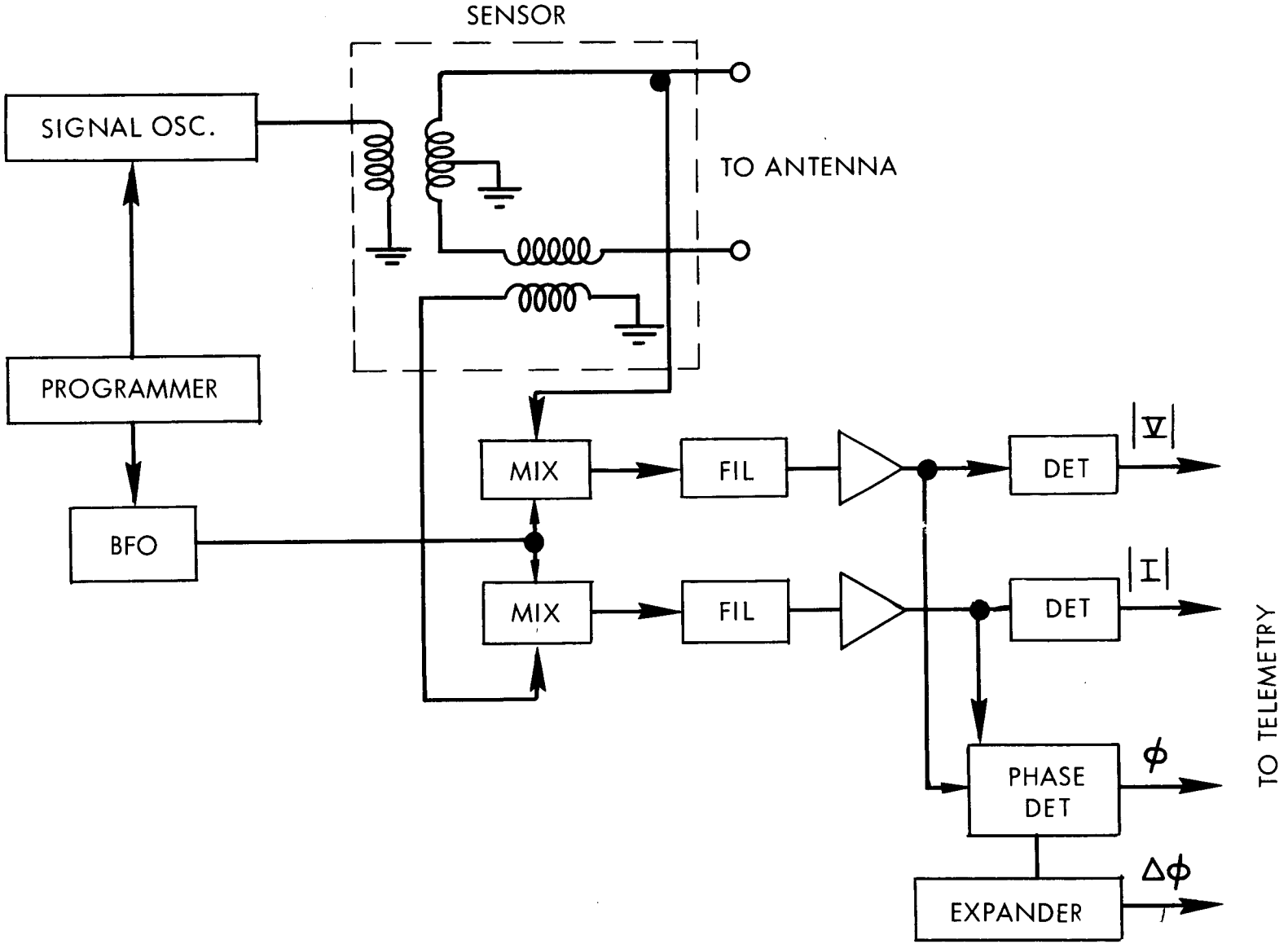
SENSOR
SIGNAL OSC.
TO ANTENNA
PROGRAMMER
BFO
MIX
FIL
DET
|V|
MIX
FIL
DET
|I|
PHASE DET
ϕ
EXPANDER
Δϕ
TO TELEMETRY

Figure 3

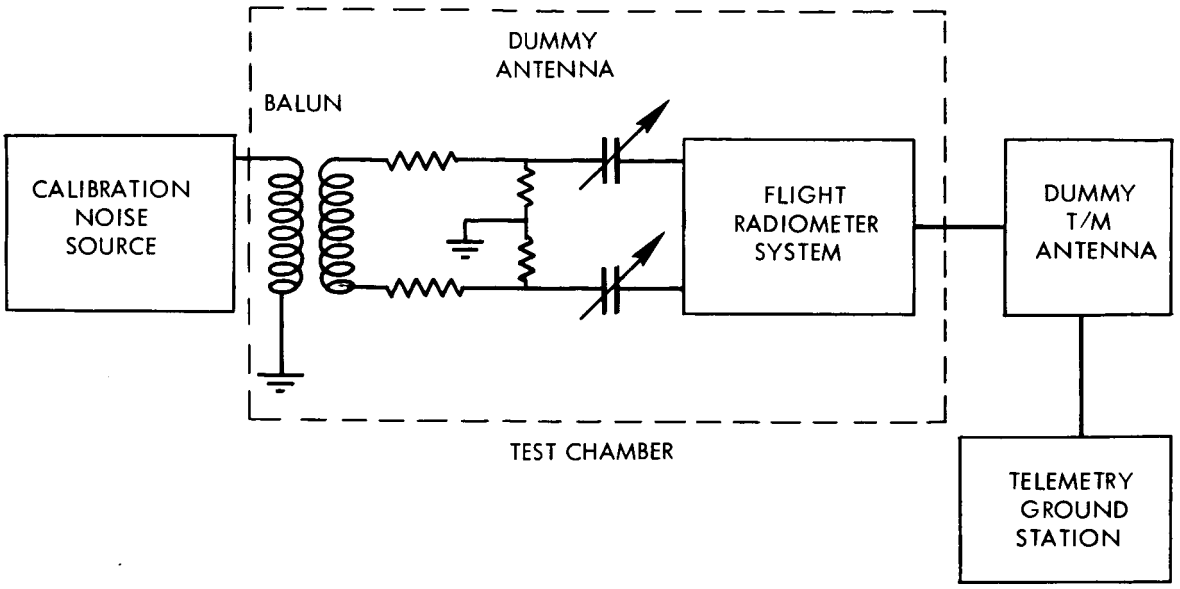

Figure 4a

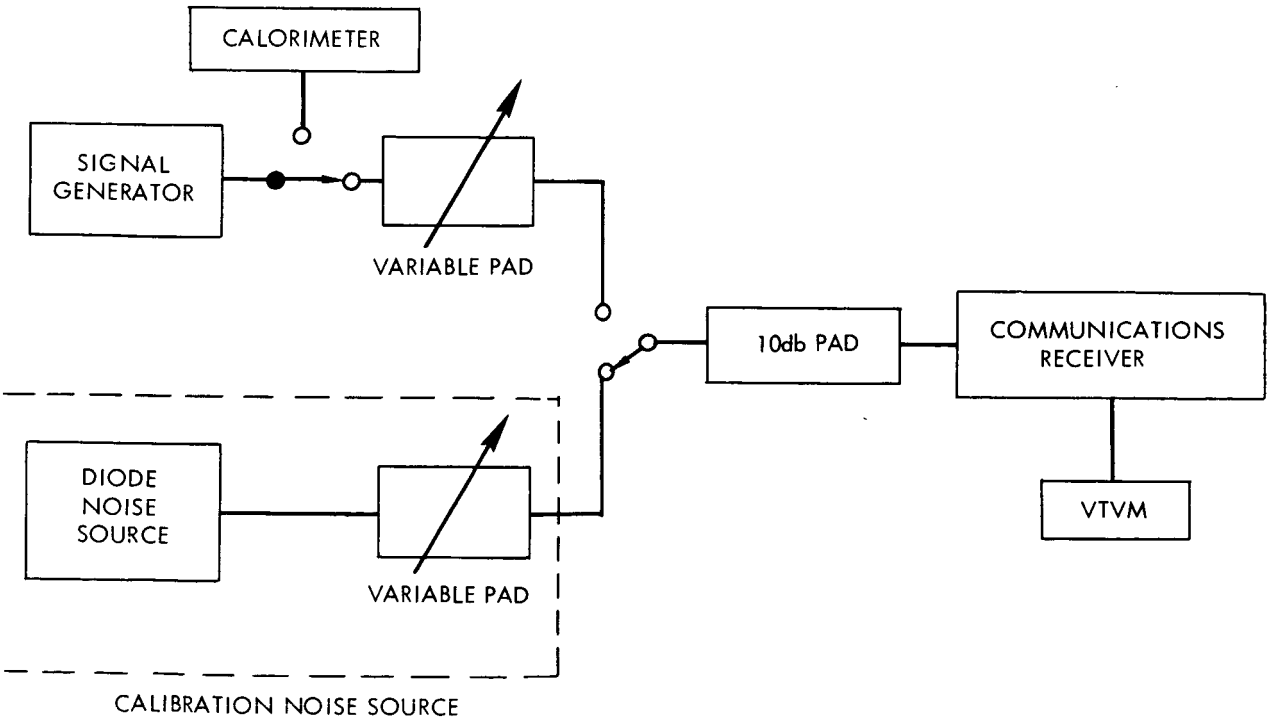

Figure 4b

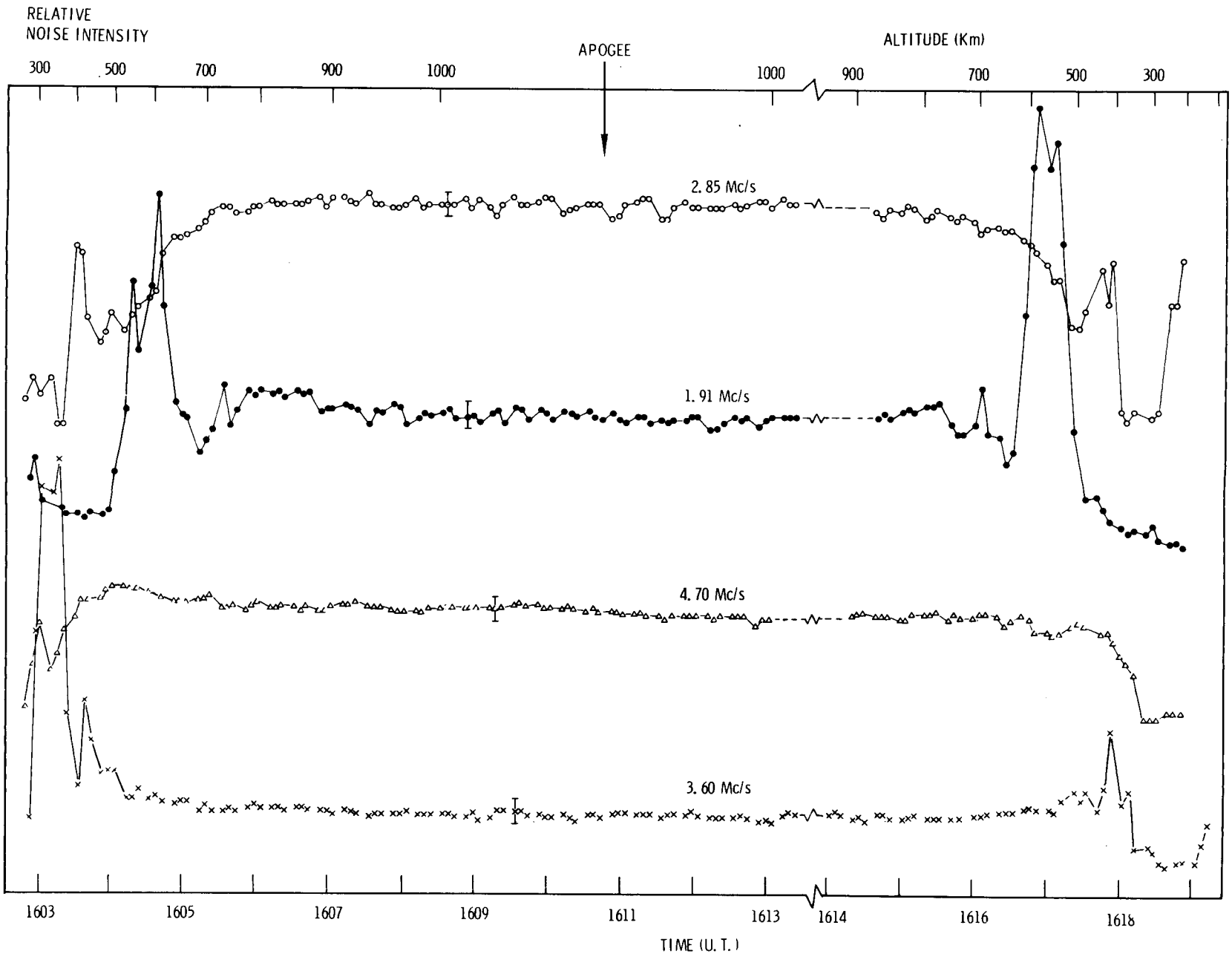
RELATIVE
NOISE INTENSITY
300
500
700
900
1000
APOGEE
1000
900
700
500
300
ALTITUDE (Km)
2.85 Mc/s
1.91 Mc/s
4.70 Mc/s
3.60 Mc/s
1603
1605
1607
1609
1611
1613
1614
1616
1618
TIME (U.T.)

Figure 5

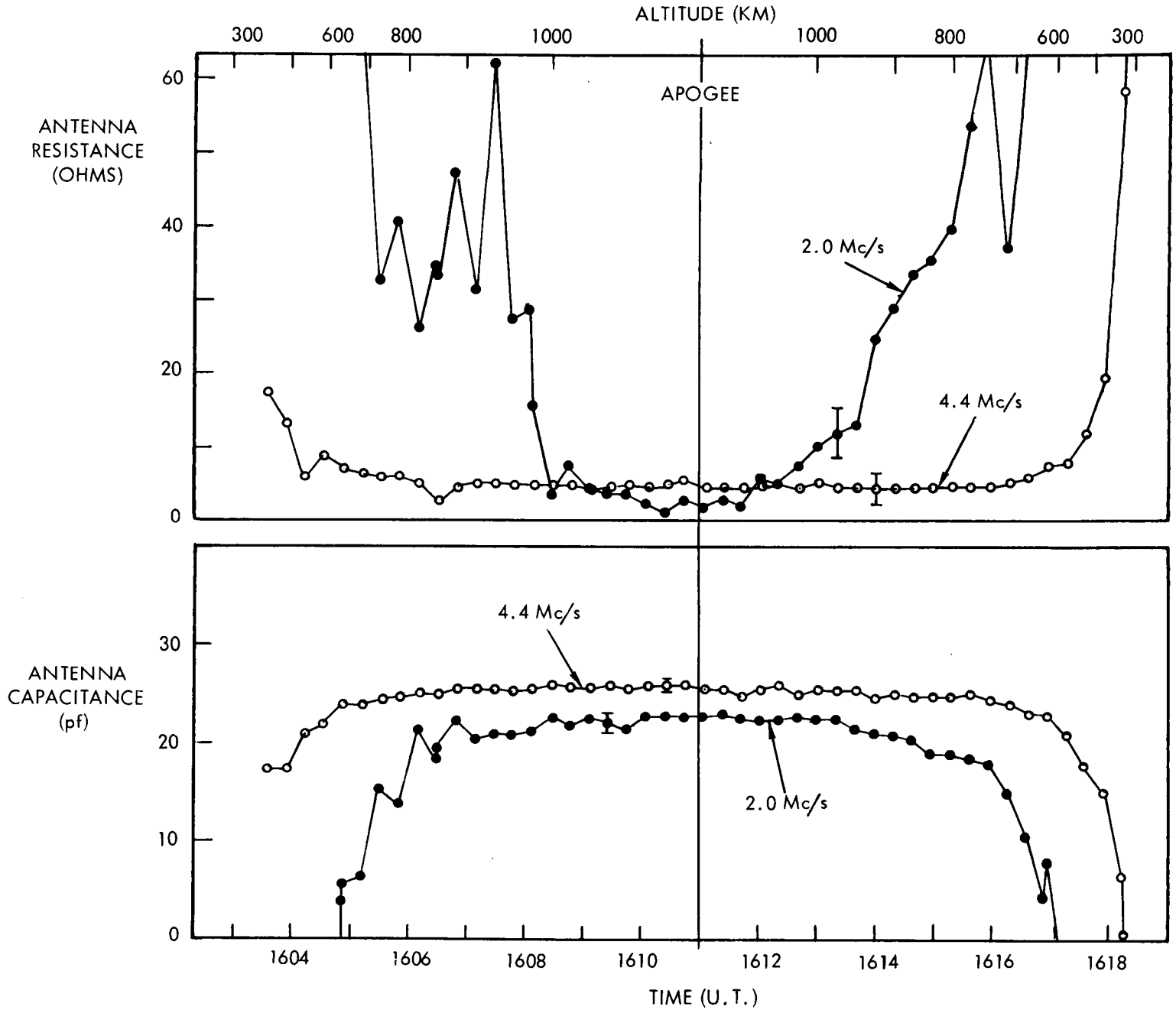
ALTITUDE (KM)
300
600
800
1000
1000
800
600
300
APOGEE
ANTENNA RESISTANCE (OHMS)
60
40
20
0
2.0 Mc/s
4.4 Mc/s
ANTENNA CAPACITANCE (pf)
30
20
10
0
4.4 Mc/s
2.0 Mc/s
1604
1606
1608
1610
1612
1614
1616
1618
TIME (U.T.)

Figure 6

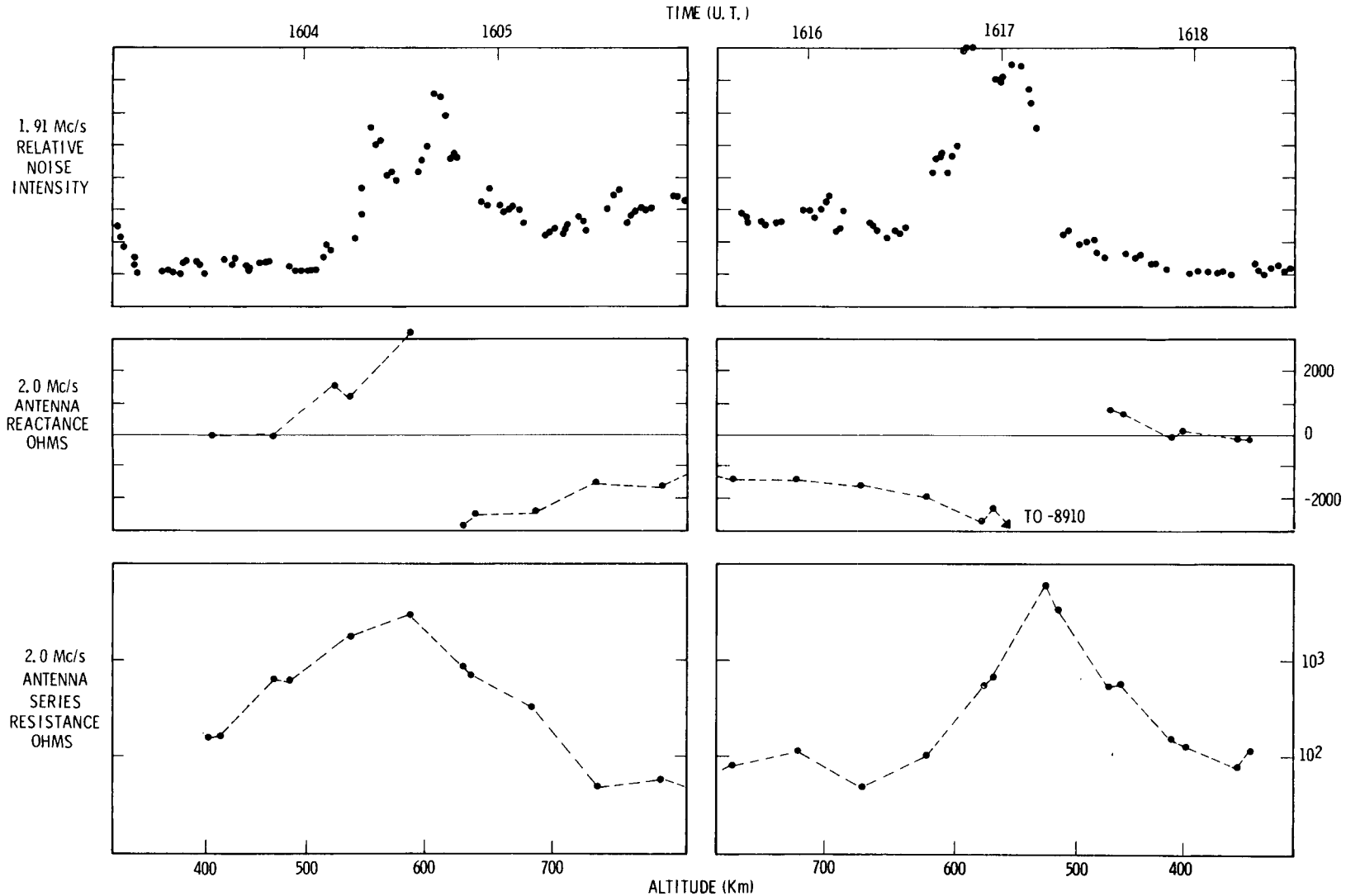
TIME (U.T.)
1604
1605
1616
1617
1618
1.91 Mc/s
RELATIVE
NOISE
INTENSITY
2.0 Mc/s
ANTENNA
REACTANCE
OHMS
2000
0
-2000
TO -8910
2.0 Mc/s
ANTENNA
SERIES
RESISTANCE
OHMS
10^3
10^2
400
500
600
700
700
600
500
400
ALTITUDE (Km)

Figure 7

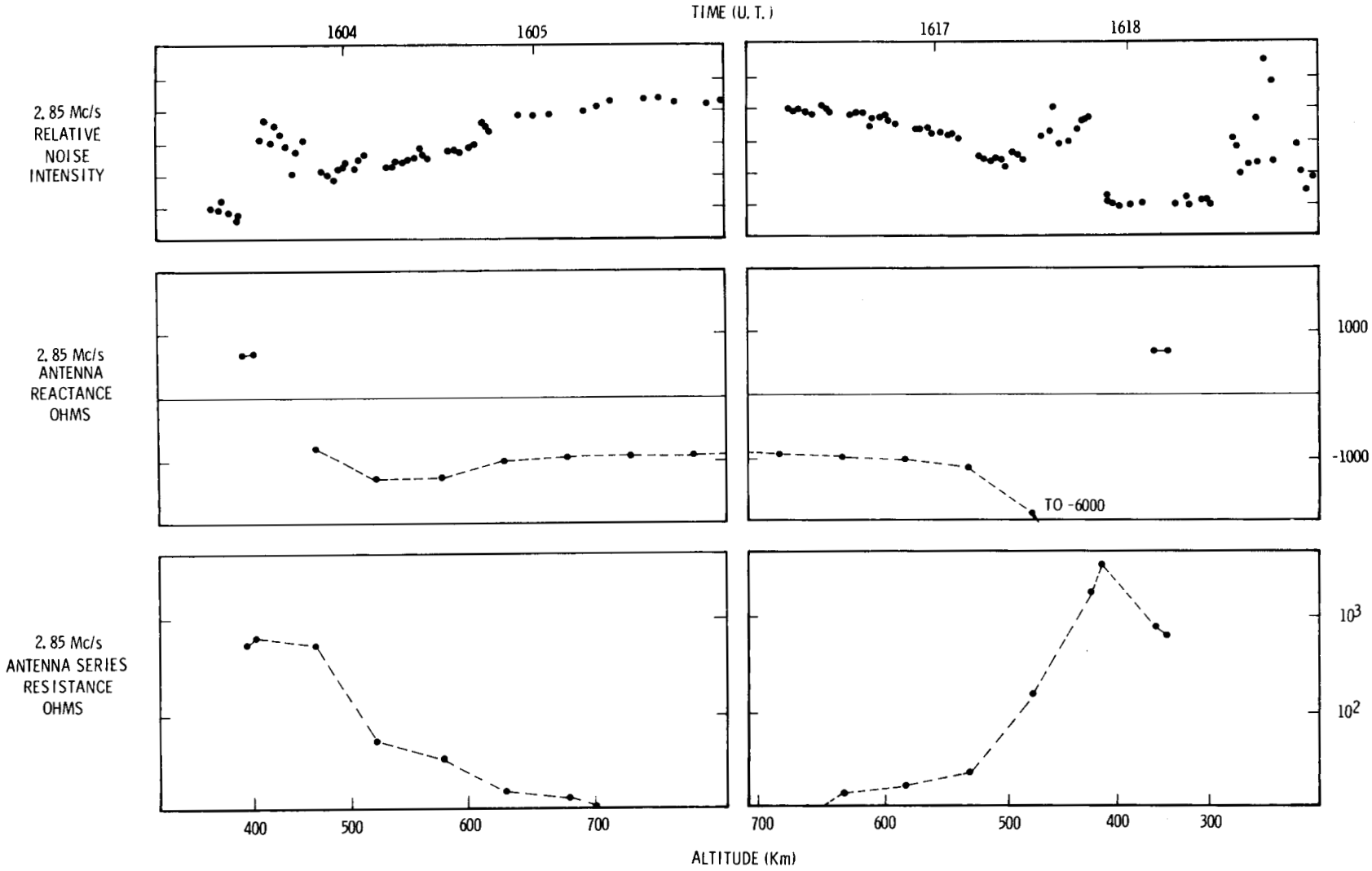
TIME (U. T.)
1604
1605
1617
1618
2.85 Mc/s
RELATIVE
NOISE
INTENSITY
2.85 Mc/s
ANTENNA
REACTANCE
OHMS
1000
-1000
TO -6000
2.85 Mc/s
ANTENNA SERIES
RESISTANCE
OHMS
10^3
10^2
400
500
600
700
700
600
500
400
300
ALTITUDE (Km)

Figure 8

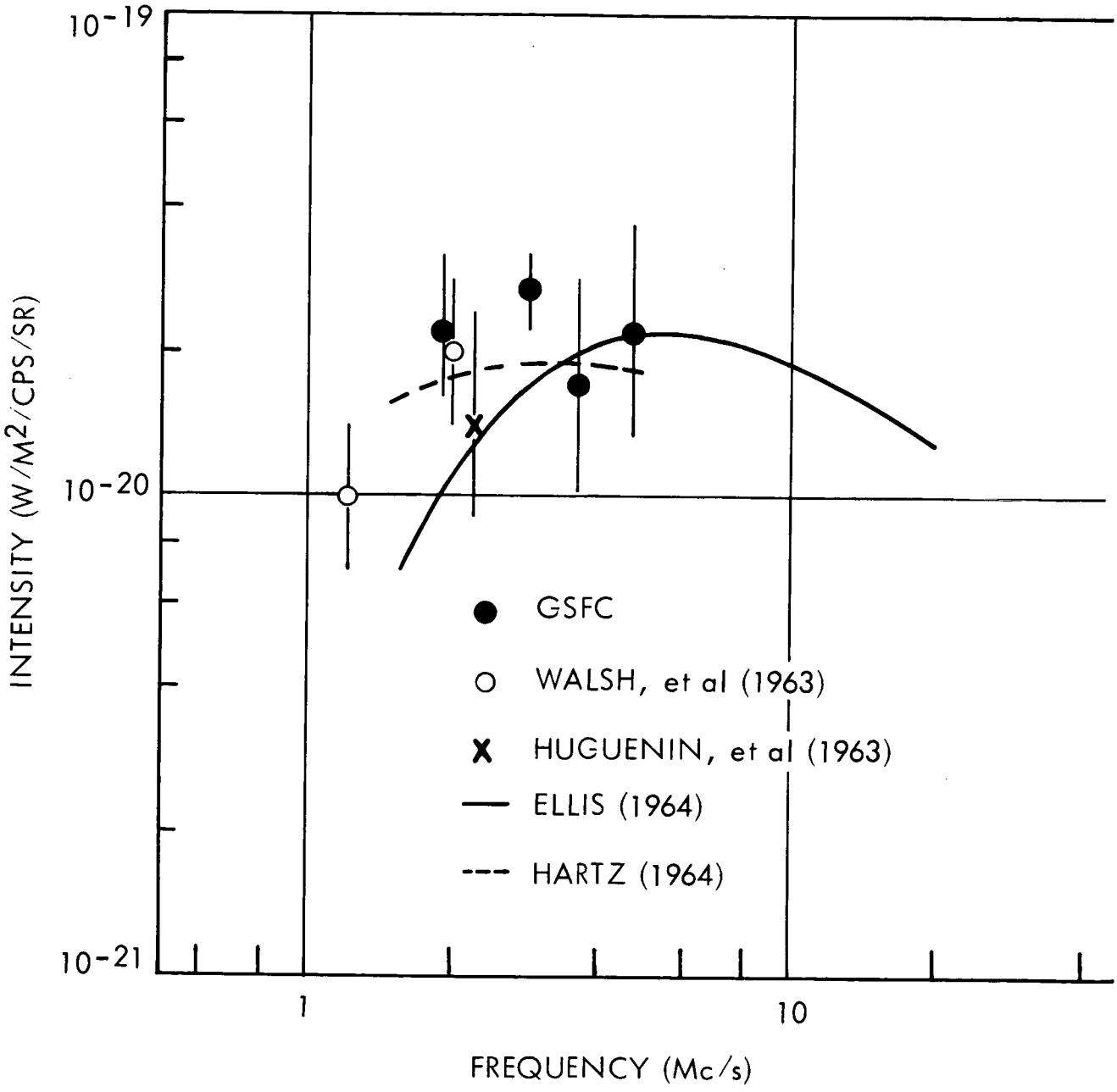
10-19
10-20
10-21
INTENSITY (W/M2/CPS/SR)
1
10
FREQUENCY (Mc/s)
GSFC
WALSH, et al (1963)
HUGUENIN, et al (1963)
ELLIS (1964)
HARTZ (1964)

Figure 9

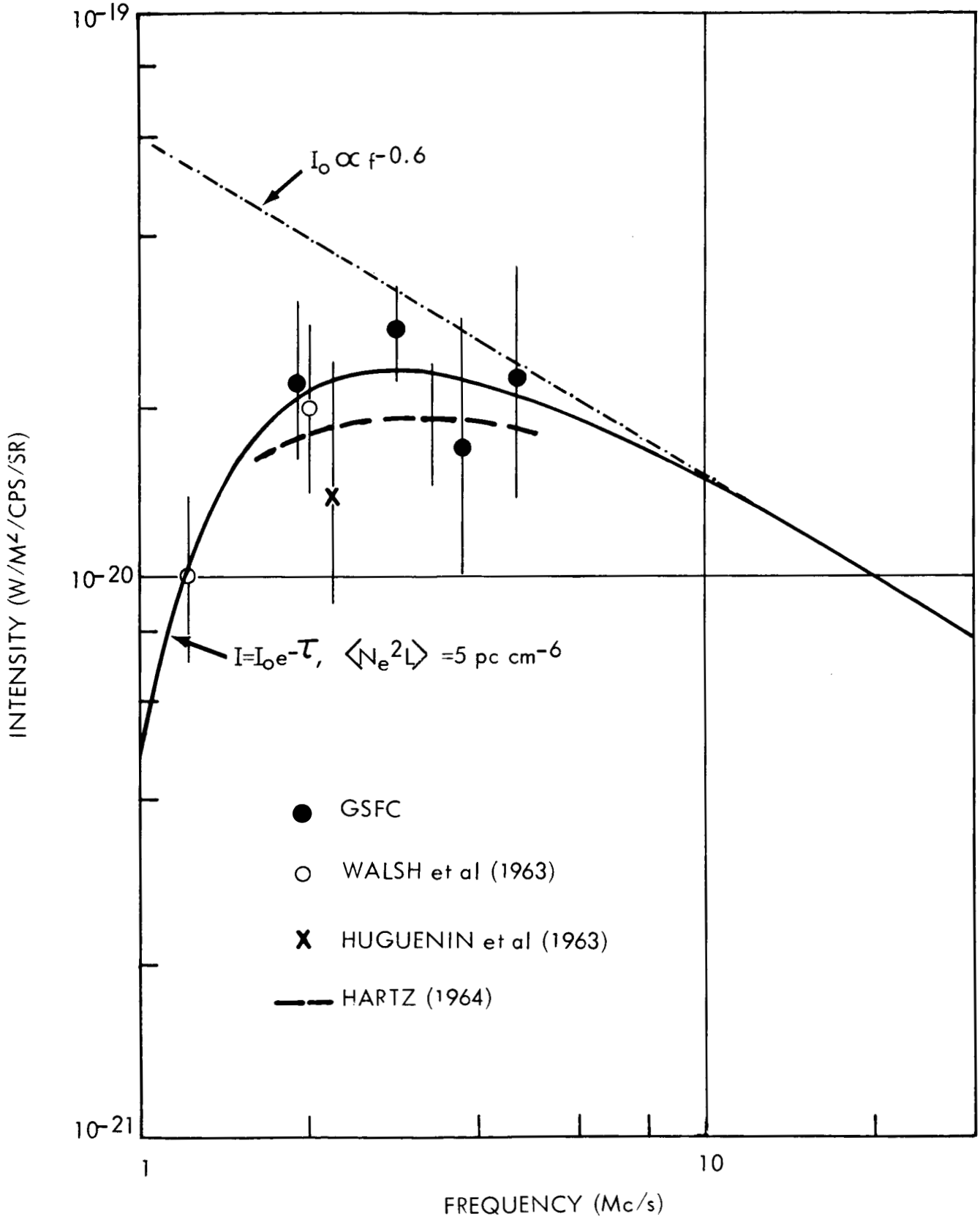
10^{-19}
$I_o \propto f^{-0.6}$
10^{-20}
$I=I_o e^{-\tau}$, $\langle N_e^2 L \rangle$ =5 pc cm^{-6}
GSFC
WALSH et al (1963)
HUGUENIN et al (1963)
HARTZ (1964)
10^{-21}
1
10
INTENSITY (W/M^2/CPS/SR)
FREQUENCY (Mc/s)

Figure 10